Ab initio molecular dynamics investigation of beryllium complexes

Onyekachi Raymond,[a,b]† Michael Bühl,[c]† Joseph R. Lane,[a] William Henderson,[a]† Penelope J. Brothers,[d] Paul G. Plieger,[e]†

[a] Chemistry, School of Science, University of Waikato, Private Bag 3105, Hamilton, New Zealand. E-mail: w.henderson@waikato.ac.nz

[b] Institute of Environmental Science and Research (ESR), PO Box 50348, Wellington, New Zealand. E-mail: onyekachi.raymond@esr.cri.nz

[c] EaStCHEM School of Chemistry, North Haugh, University of St Andrews, St. Andrews, Fife, UK, KY16 9ST. E-mail: buehl@st-andrews.ac.uk

[d] Research School of Chemistry, Australian National University, Canberra, ACT2600, Australia. E-mail: Penelope.brothers@anu.edu.au

[e] Institute of Fundamental Sciences, Massey University, Private Bag 11222, Palmerston North 4410, New Zealand. E-mail: P.G.Plieger@massey.ac.nz

† Authors to whom correspondence should be addressed

Abstract

Structures of aqueous $[Be(H_2O)_4]^{2+}$, its outer-sphere and inner-sphere complexes with F^-, Cl^- and SO_4^{2-}, as well as dinuclear complexes with a $[Be_2(\kappa\text{-}OH)(\kappa\text{-}SO_4)]^+$ core have been studied through Car-Parrinello molecular dynamics (CPMD) simulations with the BLYP functional. According to constrained CPMD/BLYP simulations and pointwise thermodynamic integration, the free energy of deprotonation of $[Be(H_2O)_4]^{2+}$ and its binding free energy with F^- are 9.6 kcal mol^{-1} and -6.2 kcal mol^{-1}, respectively, in good accord with available experimental data. The computed activation barriers for replacing a water ligand in $[Be(H_2O)_4]^{2+}$ with F^- and SO_4^{2-}, 10.9 kcal mol^{-1} and 13.6 kcal mol^{-1}, respectively, are also in good qualitative agreement with available experimental data. These ligand substitution reactions are indicated to follow associative interchange mechanisms with backside (S_N2-like) attack of the anion relative to the aquo ligand it is displacing. Outperforming static DFT computations of the salient kinetic and thermodynamic quantities involving simple polarizable continuum solvent models, CPMD simulations are validated as a promising tool to study structures and speciation of beryllium complexes in aqueous solution.

Keywords: Beryllium; Speciation; *Ab initio* molecular dynamics, CPMD, Hydrolysis.

Introduction

The greatest advantage of computational chemistry is that it enables the chemist to explore areas of scientific interest where experiments are difficult, hazardous, expensive or impossible. One such area is the chemistry of beryllium. "Microgram for microgram",[1] beryllium has been described as the most toxic element in the periodic table as a result of the uncontrollable immune response of the body's white blood cells in ~ 20% of exposed individuals subsequent to the inhalation of less than microgram portions of beryllium particles.[2-4] Consequently, this has necessitated studies on the aqueous solution chemistry of beryllium over the past two decades. A key area of interest is the solvation of the beryllium ion and its interaction with counterions in its salt solutions.[5-8] Generally, it has been observed that the actual environment of the beryllium ion in aqueous solution involves fluctuating arrangements of hydration spheres and counterions especially in the presence of anions such as fluoride and sulfate.[9-11] This information is of high importance in view of the recently proposed toxicity route to beryllium sensitization involving an accompanying ion.[12] Moreover, the formation of these beryllium complexes in aqueous solution is of interest for a variety of other applications such as in environmental detection, wet chemical recycling and processing of beryllium ores.[13, 14] Consequently, the modelling of the structure and speciation of these simple beryllium complexes in the virtual laboratory is very relevant to obtain important insights into beryllium-water and beryllium-anion interactions in a solvent environment.

In previous studies by our group, electrospray ionization mass spectrometry (ESI-MS) was explored as a safe experimental technique to obtain rich information on the speciation and coordination environment of the Be^{2+} cation in aqueous

solution.[15-18] However, a number of researchers have continually relied on computational chemistry for the "safest" investigation of beryllium chemistry given that even tiny levels of exposure have been reported to sensitise the white cells.[19] Already there exist far more computational investigations than experimental studies on the coordination chemistry of beryllium. The importance of complementing computational results with those from supporting experimental techniques and *vice versa* has been emphasized by Plieger and coworkers.[20-23]

In addition, the electrospray ionization mass spectrometric technique suffers from several unavoidable but well-documented drawbacks as a result of the change in the chemical environment as the solution species are transferred into the gas phase.[16, 24] Consequently, both solution and gas phase phenomena can be represented in a mass spectrum in varying degrees and this thereby poses a challenge in fully understanding the role of the solvent on beryllium speciation by the ESI-MS technique. In order to complement species observed by ESI-MS (and indeed other experiment results reported in the literature), we now provide detailed insights into the dynamical structure of the beryllium aqua, sulfato, chlorido and fluorido complexes as a function of the solvation environment, explored using *ab initio* molecular dynamics. By employing density functional theory (DFT) implemented in the Car-Parrinello method alongside suitable pseudopotentials, the solvent effect is modelled explicitly and further utilised to study the structure, speciation and ligand-substitution reactions of beryllium complexes in aqueous solution. In this paper, Car-Parrinello molecular dynamics (CPMD) investigations were mainly concerned with the two phenomena associated with the ESI-MS behaviour of beryllium salt solutions observed and these include the deprotonation of a coordinated water molecule and the coordination of the salt anion. While the deprotonation of a coordinated water molecule and the resultant hydrolysis product

of beryllium has been studied quite extensively, the occurrence of ion pairing in beryllium solution has received far less attention.[11, 25] Although these events are highly correlated to the charge reduction during the electrospray process, they have equally been reported in the aqueous solution chemistry of beryllium.[11]

Results and discussion

CPMD investigation of beryllium ion solvation in water and liquid ammonia

The organisation of solvent molecules around the beryllium ion has continually remained a subject of experimental and computational interest because of the small size and high charge density of this ion.[7] Following up on the pioneering CPMD/BLYP study of aqueous Be^{2+} in 31 water molecules by Marx, Sprik and Parrinello[26] two unconstrained CPMD simulations of the tetraaquaberyllium cation **1a** (Chart 1) were performed in 63 and 90 water molecules for a total of 18 ps in order to define the dynamical transition of the primary and secondary solvation around the Be^{2+} cation. The radial distribution functions, gBe-O(r) from CPMD simulation of Be^{2+} in 63 and 90 water molecules for the entire simulation period are given in Figure 1a.

In accordance with the preferred tetrahedral geometry of the beryllium ion, both simulations revealed a well demarcated first solvation shell corresponding to a sharp peak (point A) which integrates into four oxygen atoms. The average Be-O distance in the first hydration sphere was 1.647(6) Å and 1.643(4) Å for the simulation in 64 H_2O and in 90 H_2O molecules, respectively, compared to the Be-O distance of 1.66 Å which was reported in 31 water molecules.[26] Interestingly,

with the increasing number of water molecules, there is a trend of a slight shortening of the Be-O bond distances towards experimental values observed to lie between 1.60-1.63 Å.[7, 27] This highlights the subtle role of the second solvation sphere in computing the structural properties of the tetraaquaberyllium cation, as has been previously observed in static calculations.[28] CPMD simulations also revealed evidence of a well-defined second hydration sphere extending from 3.5 to 4.2 Å around the Be^{2+} cation observed at point B. As shown in Figure 2, these water molecules in the second hydration sphere are clearly organised and form a distinct hydrogen-bonded network which further stabilises the species. From the integration of this peak, 9-11 water molecules reside in the second hydration sphere of a Be^{2+} where 9 is most predominant occupation number of water molecule from the sharper peak in the Be^{2+} in 90 H_2O. While no water exchange event was observed between the first and second hydration shells, interchange events were occasionally observed following the migration of water molecules between the second and the third hydration spheres as evident in the flattening of the RDF ongoing from point B to C in Figure 1a.

Unlike the extensively studied tetraaquaberyllium complex **1a**, the sparse and inconclusive experimental details on the speciation of the beryllium ion in liquid ammonia have led to the recent reinvestigation of beryllium complexes in liquid ammonia.[29, 30] Therefore, additional CPMD simulation of Be^{2+} was performed in 67 ammonia molecules for a total of 12 ps. The Be-N radial distribution functions and their integration numbers (n(r)) are shown in Figure 1b. The first peak observed at point A (which also integrates to 4 nitrogen atoms over a range of 1.694-1.849 Å) represents the first solvation shell of ammonia with an average Be-N distance of 1.742(5) Å. This value is slightly larger than the Be-N range of 1.725-1.733 Å in the recent X ray structure of **1b** (Chart 1) but within the

range of 1.710-1.74 Å from the neutron diffraction study of $[Be(ND_3)_4]^{2+}$.[29] In comparison to the aqueous system, the Be^{2+} cation similarly structured the ammonia molecule such that a second solvation sphere can be clearly observed at point B (see Figure 1b) but with an extended distance range from 3.6 - 4.8 Å which integrates into 8-11 nitrogen atoms. This finding suggests that not all the hydrogen atoms of the primary solvation shell are involved in hydrogen bonding, reflecting a weaker hydrogen bonding network in liquid ammonia in comparison to water. Furthermore, these data have shown the CPMD/BLYP functional to be fit for purpose in describing the structural properties of beryllium complexes in solutions.

CPMD investigation of the deprotonation of the tetraaquaberyllium cation and its trimeric hydrolysis product.

The predominant species in aqueous solutions of beryllium salts at pH < 3 is the tetraaquaberyllium cation **1a** (see Chart 1). However, upon increasing the solution pH, hydrolytic reactions occur, firstly yielding the monohydroxide $[BeOH(H_2O)_3]^+$ (see equation 1) which quickly polymerises into a complex mixture of oligomeric species of varying compositions.[31]

$$\mathbf{1a} + H_2O \leftrightarrows [BeOH(H_2O)_3]^+ + H_3O^+ \quad (1)$$

Due to the availability of useful experimental data, the deprotonation of the tetraaquaberyllium cation **1a** according to equation 1, which marks the onset of the beryllium hydrolytic processes, provides an appropriate reaction for the extraction of microscopic observables for comparison with experiment and a gauge of the reliability of the CPMD methodology. Considering the strong solvation of the beryllium ion and the difference in charge between the reactant and product in

equation 1, it would be rather difficult to accurately describe the solvation effects using simple polarizable continuum models (PCMs). However, CPMD simulations which are capable of modelling solvation as an actual dynamic ensemble around the reactant and product are expected to proffer better accuracy and have been used to reproduce pK_a values with accuracies of approximately 1-4 kcal/mol.[32] Additionally, CPMD simulations have been successfully employed to reproduce the acidity constant of the uranyl(VI) hydrate $[UO_2(H_2O)_5]^{2+}$ and the dissociation mechanism of formic acid.[33, 34]

To drive the deprotonation reaction forward according to equation 1, constrained CPMD simulation was performed by taking a single O-H distance as the constrained reaction coordinate (r_1 as shown in Chart 2). Then pointwise thermodynamic integration of the Helmholtz free energy along several fixed values of r_1 was propagated as the proton was extended away from the water molecule in a slow growth from 0.97 to 1.8 Å. To ensure sufficient convergence of the mean constraint force, each new step of r_1 was started up from a previous step and the simulation was carried on for 1.5-2 ps after 0.5 ps of equilibration time similar to the level of convergence previously reported.[33] The change in Helmholtz free energy evaluated according to equation 2 afforded the free-energy profile shown in Figure 3.

$$\Delta A_{a\to b} = -\int_a^b \langle f(r_1)\rangle d(r_1) \qquad (2)$$

Along the simulation pathway at about r_1 = 1.4 Å, spontaneous proton transfer occurred on the accepting water molecule in the second hydration sphere (Chart 2) followed by the well-known shuffling of the proton in CPMD simulations.[35] Therefore in order to further prolong the reaction path, additional constraints were imposed on the two OH distances in the accepting water molecule

from this point on (as shown in Chart 2). To circumvent the slightly restrictive environment incurred from these additional constraints, the equilibration time at each integration point was thereafter increased to 1 ps. By r_1=1.8 Å, the leaving proton has effectively been transferred to a water molecule from the second hydration sphere in agreement with the values for the end-point of other similar proton transfer processes.[32-34] However, it is also worth pointing out that the end of the reaction coordinate does not correspond to the ideal standard state of infinite dilution represented by the experimental ΔG^0 term which will require continuously simulating the two product species in order to diffuse away from each other. Based on deductions from various experimental reports while at the same time considering the varying concentration and ionic strength, a recommended equilibrium constant of log β^0 = -5.4 has been pointed out for the reaction in equation 1 from which a free energy of ΔG^0= 7.4 kcal/mol can be inferred at 298 K.[36] A similar value, 7.7 kcal/mol, was also obtained in a potentiometric study of beryllium hydrolysis.[31] Comparing this to the CPMD free energy profile shown in Figure 3, the predicted difference in free energy between reactant and product taken from the near plateau region around r_1=1.6 Å is 9.6 kcal/mol. This is approximately 1.9 kcal/mol higher but still in good agreement with experimental values. The reason for the sustained rise in the free energy is perhaps due to the constraint imposed on both the other OH bonds which may hinder the reorientation of the solvation shell. Also, the accumulation of significant mean force on such additional constraints as r_1 increases and the calculated ΔA values have been previously reported.[37] Nevertheless, a plateau is apparent around r_1=1.5-1.7 Å while attempts to speed up the kinetics by firstly simulating the point at r_1 = >1.4 Å at 400 K (keeping all constraints) then restarting and running the simulation for another 2.5 ps with the

thermostat set back to 320 K yielded only free energy ΔA values ca. 0.5 kcal/mol lower compared to the previous simulation.

As a further attempt to assess the validity of the choice of reaction coordinate, a plot of the mean distance of the leaving proton (r_2) to the accepting water as a function of the constrained value r_1 was made (see Supporting Information). The desirable smooth transition of the leaving proton to the accepting water molecule with no discontinuities in the reaction pathway is observed showing that there was no rapid process that could have rendered this path unacceptable due to significant bias. However, several literature reports have shown other possible and perhaps more sophisticated reaction coordinates such as the constraining of coordination numbers, but they have equally been reported to yield very similar results.[33, 38] In practice, the greatest source of error and drawback in the present day CPMD simulation and pointwise thermodynamic integration technique of this type is related to the inherent limitation applicable to the corresponding DFT-functional as well as the inexorable finiteness of the system which forces the use of a limited number of integration points and simulation times. Nevertheless, within these limitations, the computation of the acidity constant of the tetraaquaberyllium cation **1a** within typical accuracy of DFT-based methods underscores the potential and applicability of the CPMD approach in the study of beryllium complexes in solution. This can be of value in probing other beryllium hydroxido species such as the beryllium trimer $[Be_3(OH)_3]^{3+}$.

In aqueous solution, the resultant mononuclear beryllium hydroxido species formed by the deprotonation reaction of equation 1 is short lived and quickly polymerises into a range of polynuclear hydrolysis products of which the beryllium trimer $[Be_3(OH)_3]^{3+}$ is the most commonly occurring. This species has been extensively characterised in the solid state and in the gas phase.[11, 31, 39] Employing

an unconstrained CPMD simulation, this species was immersed in a box of 90 water molecules in a simulation for 6 ps. Figure 4 displays the Be-OH bond distances of the beryllium trimer which were found to oscillate around 1.5-1.69 Å, with a mean value of 1.612(7) Å. The most obvious deduction from this simulation is the stability of the cyclic arrangement for the beryllium species which was also found intact in the gas phase by ESI-MS.[16]

CPMD investigation of Be^{2+} and counter ions in aqueous solution

For an initial study of the interaction of beryllium with the counter ions in solution the monomeric complexes shown in Chart 3 have been selected, allowing for the possibility of outer sphere or inner sphere coordination of the sulfate, chloride and fluoride anions to the metal centre. It is also worth highlighting that ESI-MS data equally pointed to the existence of these species especially the inner sphere complexes, hence a more detailed investigation of structural arrangement corresponding to the stoichiometric composition from the mass spectra is herein provided. Clearly, both coordination modes would strongly affect the structural properties and the coordination ability of the aqueous ligands. Hence detailed structural and energetics of the complexes **2** and **3** (see Chart 3) was examined. Optimized geometrical parameters of complexes **2** and **3** are collected in Tables 1 and 2 alongside available experimental data. In addition, structural data from unconstrained CPMD simulations are reported therein in the gas phase and in aqueous solution of 63 water molecules for 6 ps where the CPMD simulation in solution corresponded to a 1 mol L^{-1} $BeSO_4$, and $BeCl_2$ and BeF_2 solution in which the second halide ion was left to migrate freely in the bulk solution.

Firstly, the gas phase static optimized geometries are considered. All complexes could be characterised as minima in the gas phase and in a polarizable continuum of aqueous solution each revealing C_1 symmetry. Going from the BLYP to the B3LYP functional, Tables 1 and 2, reveals that there is a trend of a slight shortening of bond distances by ca. 0.01-0.02 Å for the Be-O bonds and by ca. 0.01-0.03 Å for the Be-X bond distances. The inner sphere coordination of the chloride, fluoride and sulfate ions evidently weakened the bonding strength of the coordinated aqua ligands as observed by their elongated Be-O distances. Also, in the complex **3a**, one of the Be-O bonds was shortened due to hydrogen bonding with the sulfato ligands. This is in agreement with an earlier reported observation that sulfate ions tend to catalyse the hydrolytic tendency of the beryllium cation in solution.[40] Also, this process serves to explain the extensive beryllium hydroxido/sulfato speciation observed in studies of aqueous beryllium sulfate solutions.[16] For the outer sphere complexes **2a-c**, the sulfate and fluoride ion provided the most structural perturbation to the tetraaquaberyllium cation **1a** which involved shortening of the Be-O bond distance of a coordinated water molecule due to hydrogen bonding to an anion in the second solvation sphere. This was followed by the lengthening of the Be-O bond distance in the remaining water molecules. However, with the chloride ion in complex **2c**, all four Be-O distances were almost equivalent, signifying a lesser disruption of the primary solvation corresponding to lesser propensity for the formation of inner sphere complexes in comparison to the other anions. Moving on to the solution phase, most of the above structural trends were retained upon solvation of complexes **2 - 3** via a polarizable continuum except that the Be-OH_2 bond distance was observed to decrease by ca. 0.03 Å (for instance compare BLYP gas and BLYP PCM for **3** in Table 2). Also, for the outer sphere beryllium complexes, shortening of the Be-O bonds due to hydrogen bonding of the

water molecule to the counter ion is diminished by ca. 0.04 A for the $[Be(H_2O)_4F]^+$ complex since solvation would greatly reduce the charge density on the fluoride ion.

Comparison of the optimization by CPMD/BLYP (denoted as Cp-opt) with other DFT methods especially BYLP reveals closely related bond distances to each other thereby lending more credence to the effectiveness of the beryllium pseudopotential used in CPMD. However, going from Cp-opt geometries to dynamic average from unconstrained CPMD simulations in the gas phase, all bond distances increased (for instance compare Cp-opt and CPMD entries in Tables 1 and 2). Also, it could be observed that the most significant bond increase occurred with the $Be \cdots X$ bond in the outer sphere complexes **2a-c**, although rearrangement of the species was not observed during the simulations. Moving on to the CPMD in aqueous solution, the radial distribution functions, gBe-O(r) from CPMD simulation of the complexes **2 - 3** are given in Figure 5. In accordance with the preferred tetrahedral geometry of the beryllium ion, RDF of species **2a-c** revealed Be-O coordination integrating to 3 suggesting that the inner sphere complex of beryllium remained stable throughout the entire simulation, without any ligand detachment. Visualisation of the simulation supported the earlier suggestion from the RDF plots that the complexes **2a-c** remained intact during the 6 ps simulation, thereby attesting to the existence of the inner sphere coordination complexes in solution involving the sulfate, fluoride and chloride anions, in agreement with experimental evidence.[8, 10, 11] However, the only structures that can be structurally compared to experiment were **3a**, **3c** and **2a, 2c**. In the solid state, the $Be \cdots OSO_3$ bond distance of the outer sphere complex in **2a** was significantly elongated by ca. 0.3 Å when immersed in solution whereas CPMD simulations in the gas phase revealed a shortening by ca. 0.1 Å. However, the solvation effect on the sulfato inner sphere complex **3a** increases the Be-OSO_3 bond distance by ca. 0.01 Å in

comparison to the values observed in the structures of the disulfato beryllium anion $[Be(SO_4)_2(H_2O)_2]^{2-}$.[41] In addition, the aqueous CPMD simulation of **3c** reveals an average Be-Cl distance of ca. 2.1 Å, in reasonable comparison to EXAFS measurements[8] at 2.2 Å, whereas static optimization employing a polarizable continuum underestimate this value by 0.27-0.3 Å depending on the functional.

The sulfate ion poses the additional complication of different possible coordination modes, cf. Chart 4. CPMD simulations reveal that κ^2-SO_4 coordination to beryllium as shown in **4a** is unstable in aqueous solution. In a simulation for 6 ps, one of the κ^2-SO_4 bonds in the complex **4a** lengthens to about 3.5 Å and eventually decoordinates from the primary solvation sphere while simultaneously letting in a water molecule from the secondary coordination sphere, which leads to the collapse of **4a** into **3a** after 4.75 ps (see Figure 6). Nevertheless, a minimum on the potential energy surface was obtained for the species **4a** in the gas phase and in the polarizable continuum model. While it has been suggested that a κ^2-SO_4 coordination to beryllium could exist in beryllium sulfate melts,[10] it is clear that chelation from the four-membered ring and the small bite size of the sulfate ion cannot compete favourably with the ion solvation, thus monodentate and bridging coordination modes are preferred. Furthermore, structural inference from the stoichiometric composition supplied by ESI mass spectra have suggested mixed beryllium sulfato/hydroxido complexes proposed as complexes **4b** and **4c** illustrating additional coordination modes of the sulfato ligands (chart 4). To investigate these species in an aqueous environment, CPMD simulation of **4b** and **4c** were followed for a total of 6 ps in solution. The sulfato ligand appeared to be quite flexible and during the first 2 ps, the κ-OSO_3 bonding mode in **4b** gradually approaches the κ^2-O_2SO_2 bonding mode in complex **4c**. Also a similar but faster

rotation of the sulfato ligands was observed in a simulation starting from **4c** but both systems remain stable and unchanged throughout the simulations. The relative stability of both complexes (with the remaining coordination site of the beryllium ion filled with aqua ligands) was then examined by employing a static calculation in the gas phase and PCM. It was observed that the structure in **4b** was relatively more stable compared to **4c** by 6.2 kcal/mol and 5.2 kcal/mol in PCM and gas phase, respectively, at the B3LYP level. This indeed hints at the preference of the monodentate coordination mode of the sulfate ion aqueous systems. In comparison to the stable bridging coordination mode of the sulfate ion, corresponding complexes employing bridging X ligands (where X is chloride and fluoride) appeared to be unstable: When CPMD simulations were started from dinuclear, doubly-bridged species such as **4b** with a four-membered rings with a bridging Be-O(H)-Be and a Be-X-Be moiety, these structures opened up to singly bridged complexes with X-Be-O(H)-Be moieties (both in the gas phase and in aqueous solution), revealing that a halide would generally coordinate to the beryllium in a monodentate fashion. This observation is entirely consistent with previously reported NMR coupling evidence which also provides no suggestion of bridging fluorides.[25]

Relative energies

To answer the question of the likelihood of outer versus inner coordination of counter ions, the affinities of the beryllium ion to the sulfate, fluoride and chloride ions were assessed by following the energetics of the sequential substitution for aqua ligands in comparison with experimental data where available. Although it is important to note that apart from the individual affinities of the counter ions towards the beryllium ion, the prevalent species in solution would be

dependent on the ion concentrations in solution. Salient data of the energetic parameters computed at various DFT levels involving static PCM optimizations and single point energy evaluations according to equation 3 (where X = F^-, Cl^-) are summarised in Tables 3 and 4.

$$[Be(H_2O)_4]^{2+} + nX \leftrightarrows [BeX_n(H_2O)_{4-n}]^{(2-n)+} + nH_2O \quad (3)$$

As expected, all anions are strongly bound in the gas phase. The simple continuum model attenuates these binding energies significantly but fails to reproduce the experimental data for X = F even qualitatively. A single F^- is computed to be unbound, whereas it has a strong affinity experimentally (see ΔG values for n = 1 in Table 3). Two or more fluorides are computed to be bound, but neither the observed binding free energies nor their trends from n = 1 to 4 are reproduced even qualitatively. This failure can almost certainly be attributed to the lack of specific H-bonding interactions in the simple PCMs. We note that single halide anions with their high charge density are very difficult targets for PCMs (microsolvated complexes with additional explicit water molecules might improve the energetics, but this was not attempted).

To go beyond the simple static PCM calculation, we have evaluated the free energies of ligand substitution on the beryllium ion in water by means of constrained CPMD simulations and pointwise thermodynamic integration. We chose reaction coordinates designed to mimic the ligand substitution of a beryllium coordinated aqua ligand by X = F^- and SO_4^{2-} ligands. This would essentially involve a transition from the outer sphere complexes **2a-b** to the inner sphere complexes **3a-b.** This technique has gained increased popularity as it is widely employed to reproduce the free binding energies of metal complexes in solution.[37, 42]

Following previous experimental and computational propositions[6, 43] modelling of the ligand substitution *via* a dissociative pathway was not attempted. Besides, preliminary CPMD simulation showed that a tri-coordinated beryllium centre tends to accept a fourth water molecule to complete its coordination within 0.5 ps of simulation. Therefore, the ligand exchange was enforced by constraining the Be-X and Be-OH_2 bond distances as reaction coordinates and fixing the difference $\Delta r = r_1 - r_2$ where r_1 = Be-X and r_2 = Be-O bonds (see Chart 5). Importantly, fixing the difference in distance is less restrictive compared to individually fixing the two distances (r_1 and r_2) simultaneously as it allows a higher degree of motion such that the true nature of the TS region can be probed (O···Be-X → O···Be···X → O-Be···X).

The ligand substitution reaction was undertaken by fixing the difference Δr at successively larger values in steps sizes of 0.3 Å and propagating the system at each point until the mean constrained force $\langle f(r) \rangle$ was sufficiently converged. The Helmholtz free energy at each point was evaluated *via* numerical integration according to equation 2. Generally, the system was found to be converged within 1.5 to 2.5 ps after 0.5 ps of equilibration time in agreement with previously reported degree of convergence from similar studies.[37, 42]

Firstly, CPMD simulations of the fluoride exchange on the beryllium cation (i.e. X=F^-) are considered. Starting from the minimum at Δr = -2.18 Å and increasing the distance difference Δr the leaving fluoride ion is gradually transferred to the outer coordination sphere. It subsequently accepts hydrogen bonds from other aqua ligands while a distant aqua ligand enters the inner coordination sphere to form a solvent-separated ion pair with beryllium while passing through a transition state at Δr = 0.21 Å. A second minimum is reached at

Δr = 2.01 Å at which the mean constraint force basically is zero. Thus, the free energy difference between the two points which constitutes the total driving force for the fluoride binding is computed to be 6.2 kcal/mol by the CPMD based approach which agrees favourably with the experimental value of 6.68 kcal/mol. It should also be noted that the CPMD simulation does not correspond to the ideal state of infinite dilution and as such the order of accord between simulation and experimental can possibly differ further. Nevertheless, the CPMD method certainly constitutes improvement over the results from static calculation employing the BLYP/PCM (compare with Table 3).

On the other hand, the above CPMD simulation is more comparable to the transition from an outer sphere complex **2b** to the inner sphere complex **3b** in the last stage of a ligand substitution process according to the Eigen-Wilkins mechanism.[7] Using a conductrimetric stopped-flow technique, the experimental activation energy barrier for this process in the aqua substitution by a fluoride has been reported as 8.9 ± 0.8 kcal/mol.[44]

By employing the CPMD approach, and assuming the outer sphere complex (at the product side in Figure 7 and equation (3)) to be set at zero, the activation energy barrier for the substitution of a water molecule by the fluoride ion is reproduced as 10.7 kcal/mol. This barrier, though a bit overestimated and somewhat uncharacteristic for GGAs, is still in good agreement with the experimental value by ca 2.5 kcal/mol, an acceptable value for calculation with the present day DFT method.

It should be noted that with pre-defined reaction coordinates (which do not necessarily have to coincide with the minimum energy reaction pathway), only an upper limit for the barrier can be given (in contrast, since the free energy is a state function, the driving force for the reaction corresponding to the difference between

the start and endpoint of our integration paths should be independent of the path followed). In order to scrutinize the reaction path for possible lower activation energy barriers, the transition state region was examined further. In principle, the simulation constraint should be flexible enough so that the system can reorient to the most favourable angle of attack although this might require much longer simulation times. To speed up any possible reorientation process CPMD simulation of the transition state at Δr = 0.21 Å was performed at 400 K for an additional 2 ps. Thereafter, the endpoint of the simulation was employed to retrace the CPMD trajectory using the same step sizes and slow growth in the positive and negative direction of the transition state while maintaining the same constraint as before. Essentially, this also provided a means to probe for any hysteresis effect which can potentially upset such constrained CPMD simulations (due to the finite integration points along the reaction path). Generally, no huge deviation from the previous simulation was observed and the resultant average activation energy barrier from both simulations was 10.9 kcal/mol.

Following the O ⋯ Be ⋯ F angles of the atoms involved in the constraint confirms that the transition state corresponds to a backside attack (that is resembling the S_N2 transition state in organic chemistry mechanism as shown in Chart 5) in which the O ⋯ Be ⋯ F angle ranges between 162-178^o. Furthermore, the transition state at Δr = 0.21 Å was again simulated using the same constraint but with the respective value for the O ⋯ Be ⋯ F angle corresponding to a frontside attack (see Chart 5). Evidently, the small size of the beryllium ion highly disfavours a potential transition state in a frontside attack and this transition state species reorients into complex **2b** within 3 ps of simulation.

Certainly, the greatest limitation of present day *ab initio* molecular dynamics simulation lies in its treatment of the electronic structure commonly

implemented by the Kohn-Sham DFT formalism of which only a couple of GGA functionals have been shown to generally provide a better description of liquid water.[45] To further investigate the effect of the functional on the activation energy barrier and driving force for the reaction, a snapshot of the complex in the transition state region with zero FE gradient at Δr = 0.21 Å, was extracted and used as a starting input to locate a transition state using static calculations and implicit solvation using the PCM model. The free energy profile for the reaction is shown in Figure 8 while the energetics of the reaction calculated by various functionals is tabulated in Table 5. On going from BLYP to B3LYP and MP2 the driving force for the reaction tend to increase by 0.3 to 0.5 kcal/mol whereas the barrier of the reaction is decreased by 0.2-0.6 kcal/mol. Comparing the CPMD results to PCM data, it can be seen that the activation energy barrier is much more overestimated than the free energy difference between the two points. While static calculations at BLYP level predicted an activation energy barrier of 12.9 kcal/mol, employing the CPMD/PTI technique with the same functional yields an activation energy of 10.9 kcal/mol which is closer to the experimental value. More disparate results between PCM and CPMD are even obtained in the calculation of the driving force of the reaction whereby the PCM static calculation pinpoints the reaction energy as 12.0 kcal/mol in comparison to 6.2 kcal/mol obtained from CPMD simulations.

From these data, it is clearly observed that the large driving force for the formation of the inner sphere complex in the gas phase would be well attenuated in solution but this is difficult to describe by simple continuum models. It must also be conceded that solvation effects are not the only concern in the computation of these beryllium complexes and the description of the electronic structure is also of high importance. For instance, the highly parameterised MO6-2X functional was found to yield a static calculation result in PCM closest to experimental results

while differing from other functionals by 0.4 – 1 kcal/mol for the activation energy barrier and 1.2 – 1.7 kcal/mol for the driving force of the reaction. This is consistent with the recommendation for this functional in the computation of thermodynamics of the main group elements.[46]

Finally, the same CPMD-based technique has been used to evaluate the activation energy barrier involved in the ligand substitution of a water molecule by the sulfate ion in the tetraquaberyllium cation **1a** using the corresponding $H_2O \cdots Be \cdots SO_4$ bond distance as reaction coordinate. In the resulting free-energy profile depicted in Figure 9a starting from the outer sphere sulfato complex $Be(H_2O)_4.SO_4$ at Δr = -2.1 Å, a second but slightly higher minimum is apparent at the end of the simulation at Δr = 1.7 Å corresponding to the inner sphere complex $BeSO_4.(H_2O)_3.H_2O$. According to Figure 9a, the activation free energy barrier for this reaction is obtained as 13.6 kcal/mol. Several measurements of the activation energy for the ligand substitution of the aqua ligand by a sulfate ion have been reported with varying degrees of agreement.[40, 47] However the activation energy barrier of 11 kcal/mol, reported by Strehlow and Knoche by employing a pressure jump relaxation technique to re-examine other previously published data appear to be more reliable.[40] CPMD simulation in this study has reproduced this the activation energy barrier within 2.6 kcal/mol.

To further investigate the effect of the solvent, the ligand substitution path of the sulfate ion for a water molecule was followed in the gas phase. Similar CPMD simulations were again set up employing the same constraint and the resultant free-energy profile is depicted in Figure 9b. Judging from the difference in ΔA between the two curves in Figure 9a and b, the stabilization of the inner sphere sulfato complex in the gas phase amounts to ca. 7.5 kcal/mol. Moreover, it can be observed that the larger driving force of the formation of the inner sphere beryllium sulfato

complex in the gas phase is attenuated in solution. This is in complete accord with the ubiquitous observation of the beryllium sulfato complex in the ESI-MS of beryllium sulfate solution and is further agreement of the proposed route of charge reduction during the ESI-MS process. Additionally, it is should also be noted that the substitution of the aqua ligand by a sulfato ligand is catalysed by the OH^- ion thereby suggesting other pathways leading to the inner sphere complex.[40]

Mechanism of counterion exchange process with an aqua ligand on the solvated beryllium cation

The water exchange on the tetraaquaberyllium cation **1a** has previously been studied both experimentally and computationally in some detail.[6, 7, 43] The consensus classification for the water exchange between the first and second coordination spheres of the beryllium ion with aqua ligand is a limiting associative or associative interchange mechanism according to the high negative activation volume of -13.6 cm^3 mol^{-1} relative to other water exchange processes. On the other hand, computational results of Puchta *et al* appear to provide evidence for the interchange mechanism as predominant in water exchange.[48] This result is consistent with previous mechanistic studies involving water exchanges. Computationally, the preference for a mechanism is often rationalized by examining key species, especially the transition state species. For the substitution mechanisms for simple ligands such as fluoride ions on $[Be(H_2O)_4]^{2+}$, tracing the reaction energy trajectory for the exchange mechanism by the CPMD/PTI technique passes through a trigonal bipyramidal penta-coordinated complex. The occurrence of the transition state at Δr close to zero points out that both the entering and the leaving groups have considerable bonding to the beryllium centre which is

a clear indication of an interchange type of mechanism. Realistically, an interchange associative Ia mechanism would be challenging to distinguish from an interchange mechanism. However, while the associative mechanism produces an intermediate of which all the bonds to the beryllium ion are within the expected range as in the reactants and products and thus can be characterized by the absence of any imaginary vibrational frequency the interchange mechanism reveals a transition state. The static optimization of this trigonal bipyramidal penta-coordinated beryllium complex for the fluoride exchange could be characterized as a true transition state by the presence of exactly one imaginary vibrational frequency when optimized with the B3LYP functional in agreement with an interchange associative mechanism.

Furthermore, it is obvious that the small size of the beryllium ion will strongly disfavour a five coordinate species with similar bond distances as would be required to form a true intermediate. Rather, inspection of the Be-O and Be-X ($X=F^-$, SO_4^{2-}) bond distances of the entering and leaving ligands reveal that their bond distances are 0.3-0.8 Å longer than the Be-O/Be-X bonds not directly involved in the exchange process. This is more obvious with the sulfate exchange compared to the fluoride ion possibly due to steric factors. However, for the sulfate substitution, attempts to optimize a transition state failed repeated times though this does not connote the absence of a transition state. Obviously, the agreement of the CPMD results from this study with experimental data reveal that the mechanism for the fluoride and sulfate substitution with aqua ligands proceed via an interchange mechanism.

Conclusion

In summary, we have employed static DFT calculations and Car-Parrinello molecular dynamics simulations to elucidate the precise coordination environment about the beryllium ion in mixed aquo, fluorido and sulfato complexes as proposed from stoichiometry data assessed from electrospray ionization mass spectrometry. It was established that in the presence of counter ions such as fluoride, sulfate and chloride, inner sphere complexes exist in solution in agreement with the observation made in earlier discussed mass spectra. The sulfate and fluoride ions were particularly prone to the formation of such species in comparison to the chloride ion. In addition, the multidentate nature of the sulfate facilitated various polynuclear structural arrangements of beryllium sulfato complexes. Furthermore, the role of the solvation on geometric and energetic parameters of beryllium complexes were illustrated pointing out that the accurate description of the solvent effect is particularly challenging for simple continuum models. On the other hand, the computationally demanding technique of *ab initio* molecular dynamics, involving the treatment of the whole solution as a dynamic ensemble has provided better agreement with experimental data thereby highlighting the role played by the hydrogen bond interactions with the solute which are critical but which, unfortunately, cannot be captured by a continuum. Finally, it has been shown that the beryllium speciation in aqueous solution could involve independent hydrated metal ions as well as inner and outer sphere complexes depending on the binding affinity of the counterion and its concentration in solution. This insight into the speciation of beryllium in a solvent environment using the CPMD/PTI methodology as well as the impressive reproduction of the energetics of the ligand substitution reaction on the beryllium cation would be a reference point in

subsequent *ab initio* molecular dynamics simulations of beryllium interactions with important binding sites on other ligands of interest.

Computational details

Static calculations

Static calculations on the beryllium complexes were performed using the Gaussian 09 program.[49] Non-periodic geometry optimizations using density functional theory (DFT) were performed in the gas phase and aqueous phase employing the PCM implementation of Tomasi and co-workers[50] (utilising the united-atom UFF radii and the parameters of water). The main DFT functional employed for the calculation of the exchange-correlation energy were the BLYP[51, 52] and the hybrid B3LYP[52, 53] functionals. These were chosen in order to assess a close comparison with results from *ab initio* molecular dynamics simulations. The minimum or the transition state character of each geometry was verified by computation of the harmonic vibrational frequencies. Thereafter, using the optimized geometries from the respective medium, single point energies were calculated both in gas phase and the PCM with 6-311++G(d,p) basis. Gibbs free energy differences were obtained by subtracting reactant from the free energies of the products. In addition, the effect of empirical dispersion corrections of Grimme and the basis-set superposition error (BSSE) (evaluated using the counterpoise method) on individual bonds were computed.[54]

Ab initio molecular dynamics

Ab initio molecular dynamics were performed using the Car-Parrinello scheme[55] as implemented in the CPMD program[56] (version 3.7). CPMD simulations were

performed using the BLYP functional as this functional has been noted to display impressive performance in describing the properties of liquid water.[57, 58] Norm conserving pseudopotentials utilised in this study were generated according to the procedure by Troullier and Martins[59] and transformed into the nonlocal form using the scheme proposed by Kleinman-Bylander.[60] A new pseudopotential was generated for beryllium (see Supporting Information) while the pseudopotential employed for all other elements had been previously generated and validated.[42] Geometric parameters labelled as CP-opt involved optimization implemented in the CPMD program until the maximum gradient was less than $5x10^{-4}$ a.u.

The electronic wave functions were described using the Kohn-Sham orbitals expanded in plane waves up to a kinetic energy cut-off of 80 Ry. The simulations were performed in a periodically repeating cubic box with lattice constant varying depending on the size of the system. While a cell edge of 12.8 Å was employed for simulation of the beryllium species in the gas phase or in a box of 67 water molecules, 14 Å was employed for the simulations in 90 water molecules. Starting structures involving 67 water molecules were generated from a pre-equilibrated system from previous CPMD simulations[42] (by manually placing in the appropriate atoms with the Be complex) while the water molecules in the bigger box were generated from pre-equilibrated classical MD snapshots.

The CPMD simulations were performed with a fictitious electronic mass of 600 a.u, and a time step of 0.0121 fs, in a NVT ensemble using a single Nosé-Hoover thermostat set to 300 K (instantaneous heat-up, frequency 1800 cm^{-1}), except when otherwise stated (in order to increase the mobility of the solvent). Hydrogen was substituted with deuterium in order to increase the time step and long-range electrostatic interactions treated with the Ewald method,[5] electrostatic

decoupling between the cell was exempted since the error introduced in a related system have been reported to be insignificant.

Unconstrained CPMD were generally performed over 6-18 ps and the first 3 ps were taken for equilibration. Furthermore, constrained CPMD simulation in the gas phase and aqueous solution were conducted along defined reaction coordinates. Thereafter, pointwise thermodynamic integration (PTI)[61] of the mean constraint force along the chosen coordinates were evaluated to obtain the changes in the Helmholtz free energy according to equation 2 and at each point, the simulation was performed until the mean constraint force was converged.

ACKNOWLEDGMENTS

We thank EaStCHEM and the School of Chemistry in St Andrews for support. Calculations were performed on local Opteron clusters maintained by Dr. H. Früchtl and on a Silicon Graphics cluster at UCL, where a generous CPU grant from the National Service for Computational Chemistry Software is gratefully acknowledged. OR thanks the Marsden Fund of the New Zealand Government (contract MAU1204), administered by the Royal Society of New Zealand for financial support of this work.

References

1. Newman, L. S., Beryllium. *Chemical & Engineering News* **2003**, http://pubs.acs.org/cen/80th/beryllium.html. Accessed June 2017.

2. McCleskey, T. M.; Scott, B. L., Beryllium and strong hydrogen bonds. *J. Occup. Env. Hyg.* **2009,** *6* (12), 751-757.

3. Schroeder, H. A., The role of trace elements in cardiovascular diseases. *Med. Clin. North Am.* **1974,** *58* (2), 381-396.

4. Borak, J., Chronic Beryllium Disease: The Search for a Dose-Response. *J. Occup. Environ. Med.* **2016,** *58* (11), e355-e361.

5. Toukmaji, A. Y.; Board, J. A., Ewald summation techniques in perspective: a survey. *Comput. Phys. Commun.* **1996,** *95* (2-3), 73-92.

6. Puchta, R.; Pasgreta, E.; van Eldik, R., Ligand exchange processes on the smallest solvated alkali and alkaline earth metal cations: an experimental and theoretical approach. *Adv. Inorg. Chem.* **2009,** *61*, 523-571.

7. Richens, D. T., *The Chemistry of Aqua Ions: Synthesis, Structure, and Reactivity : A Tour Through the Periodic Table of the Elements*. Wiley: Chichester, 1997.

8. Mason, P. E.; Ansell, S.; Neilson, G. W.; Brady, J. W., Be2+ hydration in concentrated aqueous solutions of $BeCl_2$. *J. Phys. Chem. B* **2008,** *112* (7), 1935-1939.

9. Rudolph, W. W., Raman and infrared spectroscopic investigation of speciation in $BeSO_4$ (aq). *J. Solution Chem.* **2010,** *39* (7), 1039-1059.

10. Rudolph, W. W.; Fischer, D.; Irmer, G.; Pye, C. C., Hydration of beryllium (II) in aqueous solutions of common inorganic salts. A combined vibrational spectroscopic and ab initio molecular orbital study. *Dalton Trans.* **2009,** (33), 6513-6527.

11. Alderighi, L.; Gans, P.; Stefeno, M.; Vacca, A., Aqueous Solution Chemistry of Beryllium. In *Adv. Inorg. Chem.*, Sykes, A. G.; Cowley, A., H, Eds. Academic Press: California, 2000; Vol. 50, 109-197.

12. Clayton, G. M.; Wang, Y.; Crawford, F.; Novikov, A.; Wimberly, B. T.; Kieft, J. S.; Falta, M. T.; Bowerman, N. A.; Marrack, P.; Fontenot, A. P., Structural basis of chronic beryllium disease: linking allergic hypersensitivity and autoimmunity. *Cell* **2014,** *158* (1), 132-142.

13. Brisson, M. J.; Ekechukwu, A. A., *Beryllium: Environmental Analysis and Monitoring*. Royal Society of Chemistry: United Kingdom, 2009.

14. Walsh, K. A.; Vidal, E. E., *Beryllium Chemistry and Processing*. ASM International: Ohio, 2009.

15. Raymond, O.; Brothers, P. J.; Buchner, M. R.; Lane, J. R.; Müller, M.; Spang, N.; Henderson, W.; Plieger, P. G., Electrospray Ionization Mass Spectrometric Study of the Gas-Phase Coordination Chemistry of Be2+ Ions with 1, 2-and 1, 3-Diketone Ligands. *Inorg. Chem.* **2019,** *58* (9), 6388-6398.

16. Raymond, O.; Henderson, W.; Brothers, P. J.; Plieger, P. G., Electrospray Ionisation Mass Spectrometric (ESI MS) Investigation of Beryllium Hydrolysis in Acidic Solutions of Beryllium Sulfate. *Eur. J. Inorg. Chem.* **2017,** *2017* (20), 2691-2699.

17. Raymond, O.; Henderson, W.; Brothers, P. J.; Plieger, P. G., Electrospray Ionisation Mass Spectrometric (ESI MS) Screening and Characterisation of Beryllium Complexes with Potentially Encapsulating Aminopolycarboxylate and Related Ligands. *Eur. J. Inorg. Chem.* **2018,** *2018* (9), 1120-1130.

18. Raymond, O.; Perera, L. C.; Brothers, P. J.; Henderson, W.; Plieger, P. G., The Chemsitry and Metallurgy of Beryllium. *Chemistry in New Zealand* **2015,** *79* (3), 137-143.

19. Infante, P. F.; Newman, L. S., Beryllium exposure and chronic beryllium disease. *The Lancet* **2004,** *363* (9407), 415-416.

20. Agrawal, A.; Cronin, J.; Tonazzi, J.; McCleskey, T. M.; Ehler, D. S.; Minogue, E. M.; Whitney, G.; Brink, C.; Burrell, A. K.; Warner, B., Validation of a standardized portable fluorescence method for determining trace beryllium in workplace air and wipe samples. *J. Environ. Monit.* **2006,** *8* (6), 619-624.

21. Plieger, P. G.; John, K. D.; Burrell, A. K., Encapsulating beryllium–Synthesis, characterisation and modelling of a chiral binaphthyldiimine-Be (II) complex. *Polyhedron* **2007,** *26* (2), 472-478.

22. Plieger, P. G.; John, K. D.; Keizer, T. S.; McCleskey, T. M.; Burrell, A. K.; Martin, R. L., Predicting ^{9}Be nuclear magnetic resonance chemical shielding tensors utilizing density functional theory. *J. Am. Chem. Soc.* **2004,** *126* (44), 14651-14658.

23. Shaffer, K. J.; Davidson, R. J.; Burrell, A. K.; McCleskey, T. M.; Plieger, P. G., Encapsulation of the BeII Cation: Spectroscopic and Computational Study. *Inorg. Chem.* **2013,** *52* (7), 3969-3975.

24. Cole, R. B., *Electrospray and Maldi Mass Spectrometry:Fundamentals, Instrumentation, Practicalities, and Biological Applications*. 2nd ed.; Wiley: New Jersey, 2010.

25. Schmidbaur, H., Recent contributions to the aqueous coordination chemistry of beryllium. *Coord. Chem. Rev.* **2001,** *215* (1), 223-242.

26. Marx, D.; Sprik, M.; Parrinello, M., Ab initio molecular dynamics of ion solvation. The case of Be^{2+} in water. *Chem. Phys. Lett.* **1997,** *273* (5), 360-366.

27. Massa, W.; Dehnicke, K., $[Be(OH_2)_4]Cl^{2-}$ Herstellung, IR Spektrum und Kristallstruktur. *Z. Anorg. Allg. Chem.* **2007,** *633* (9), 1366-1370.

28. Bock, C. W.; Glusker, J. P., Organization of water around a beryllium cation. *Inorg. Chem.* **1993,** *32* (7), 1242-1250.

29. Kraus, F.; Baer, S. A.; Buchner, M. R.; Karttunen, A. J., Reactions of Beryllium Halides in Liquid Ammonia: The Tetraammineberyllium Cation $[Be(NH_3)_4]^{2+}$, its Hydrolysis Products, and the Action of Be^{2+} as a Fluoride Ion Acceptor. *Chem. Eur. J.* **2012,** *18* (7), 2131-2142.

30. Kraus, F.; Baer, S. A.; Hoelzel, M.; Karttunen, A. J., $[Be(ND_3)_4]Cl_2$: Synthesis, Characterisation and Space Group Determination Guided by Solid‐State Quantum Chemical Calculations. *Eur. J. Inorg. Chem.* **2013,** *2013* (24), 4184-4190.

31. Schwarzenbach, G.; Wenger, H., Die Deprotonierung von Metall Aquoionen I.: $Be \cdot aq^{2+}$ Solvatations Isomerie. *Helv. Chim. Acta* **1969,** *52* (3), 644-665.

32. Trout, B. L.; Parrinello, M., The dissociation mechanism of H_2O in water studied by first-principles molecular dynamics. *Chem. Phys. Lett.* **1998,** *288* (2), 343-347.

33. Bühl, M.; Kabrede, H., Acidity of Uranyl(VI) Hydrate Studied with First Principles Molecular Dynamics Simulations. *ChemPhysChem* **2006,** *7* (11), 2290-2293.

34. Lee, J.-G.; Asciutto, E.; Babin, V.; Sagui, C.; Darden, T.; Roland, C., Deprotonation of Solvated Formic Acid: Car Parrinello and Metadynamics Simulations. *J. Phys. Chem. B* **2006,** *110* (5), 2325-2331.

35. Marx, D., Proton transfer 200 years after von Grotthuss: Insights from ab initio simulations. *ChemPhysChem* **2006,** *7* (9), 1848-1870.

36. Baes, C. F.; Mesmer, R. E., *Hydrolysis of cations*. Wiley: New York, 1976.

37. Bühl, M.; Sieffert, N.; Golubnychiy, V.; Wipff, G., Density functional theory study of uranium (VI) aquo chloro complexes in aqueous solution. *J. Phys. Chem. A* **2008,** *112* (11), 2428-2436.

38. Sprik, M., Computation of the pK of liquid water using coordination constraints. *Chem. Phys.* **2000,** *258* (2), 139-150.

39. Perera, L. C.; Raymond, O.; Henderson, W.; Brothers, P. J.; Plieger, P. G., Advances in beryllium coordination chemistry. *Coord. Chem. Rev.* **2017,** *352*, 264-290.

40. Strehlow, H.; Knoche, W., On the mechanism of ligand substitution in weak complexes. *Ber. Bunsen-Ges. Phys. Chem.* **1969,** *73* (5), 427-432.

41. Georgiev, M.; Wildner, M.; Stoilova, D.; Karadjova, V., Potassium beryllium sulfate dihydrate, $K_2 Be(SO_4)_2 \cdot 2H_2O$: Crystal structure and infrared spectroscopy. *J. Mol. Struct.* **2005,** *753* (1), 104-112.

42. Bühl, M.; Sieffert, N.; Wipff, G., Density functional study of aqueous uranyl(VI) fluoride complexes. *Chem. Phys. Lett.* **2009,** *467* (4), 287-293.

43. Pittet, P. A.; Elbaze, G.; Helm, L.; Merbach, A. E., Tetrasolventoberyllium (II): high-pressure evidence for a sterically controlled solvent-exchange mechanism crossover. *Inorg. Chem.* **1990,** *29* (10), 1936-1942.

44. Baldwin, W.; Stranks, D., Rates of substitution of the hydrated beryllium cation by hydrogen fluoride and fluoride ion. *Aust. J. Chem.* **1968,** *21* (9), 2161-2173.

45. Bankura, A.; Carnevale, V.; Klein, M. L., Hydration structure of salt solutions from ab initio molecular dynamics. *J. Chem. Phys.* **2013,** *138* (1), 014501.

46. Zhao, Y.; Truhlar, D. G., The M06 suite of density functionals for main group thermochemistry, thermochemical kinetics, noncovalent interactions, excited states, and transition elements: two new functionals and systematic testing of four M06-class functionals and 12 other functionals. *Theor. Chem. Acc.* **2008,** *120* (1-3), 215-241.

47. Strehlow, H.; Kalarickal, S., Über eine neue Temperatursprungmethode zur Messung schneller chemischer Reaktionen. *Ber. Bunsen-Ges. Phys. Chem.* **1966,** *70* (2), 139-143.

48. Puchta, R.; van Eikema Hommes, N.; van Eldik, R., Evidence for Interchange Ligand Exchange Processes on Solvated Beryllium Cations. *Helv. Chim. Acta* **2005,** *88* (5), 911-922.

49. Frisch, M. J.; Trucks, G. W.; Schlegel, H. B.; Scuseria, G. E.; Robb, M. A.; Cheeseman, J. R.; Scalmani, G.; Barone, V.; Mennucci, B.; Petersson, G. A.; Nakatsuji, H.; Caricato, M.; Li, X.; Hratchian, H. P.; Izmaylov, A. F.; Bloino, J.; Zheng, G.; Sonnenberg, J. L.; Hada, M.; Ehara, M.; Toyota, K.; Fukuda, R.; Hasegawa, J.; Ishida, M.; Nakajima, T.; Honda, Y.; Kitao, O.; Nakai, H.; Vreven, T.; Montgomery Jr., J. A.; Peralta, J. E.; Ogliaro, F.; Bearpark, M. J.; Heyd, J.; Brothers, E. N.; Kudin, K. N.; Staroverov, V. N.; Kobayashi, R.; Normand, J.; Raghavachari, K.; Rendell, A. P.; Burant, J. C.; Iyengar, S. S.; Tomasi, J.; Cossi, M.; Rega, N.; Millam, N. J.; Klene, M.; Knox, J. E.; Cross, J. B.; Bakken, V.; Adamo, C.; Jaramillo, J.; Gomperts, R.; Stratmann, R. E.; Yazyev, O.; Austin, A. J.; Cammi, R.; Pomelli, C.; Ochterski, J. W.; Martin, R. L.; Morokuma, K.; Zakrzewski, V. G.; Voth, G. A.; Salvador, P.; Dannenberg, J. J.; Dapprich, S.; Daniels, A. D.; Farkas, Ö.; Foresman, J. B.; Ortiz, J. V.; Cioslowski, J.; Fox, D. J., **2009**, Gaussian 09, Revision D. 01, Gaussian Inc., Wallingford, CT.

50. Tomasi, J.; Mennucci, B.; Cammi, R., Quantum mechanical continuum solvation models. *Chem. Rev.* **2005,** *105* (8), 2999-3094.

51. Becke, A. D., Density-functional exchange-energy approximation with correct asymptotic behavior. *Phys. Rev. A* **1988,** *38* (6), 3098-3100.

52. Lee, C.; Yang, W.; Parr, R. G., Development of the Colle-Salvetti correlation-energy formula into a functional of the electron density. *Physical review B* **1988,** *37* (2), 785-789.

53. Becke, A. D., A new mixing of Hartree – Fock and local density functional theories. *J. Chem. Phys* **1993,** *98* (2), 1372-1377.

54. Grimme, S., Density functional theory with London dispersion corrections. *Wiley Interdisciplinary Reviews: Computational Molecular Science* **2011,** *1* (2), 211-228.

55. Car, R.; Parrinello, M., Unified approach for molecular dynamics and density-functional theory. *Phys. Rev. Lett.* **1985,** *55* (22), 2471-2474.

56. Hutter, J.; Alavi, A.; Deutsch, T.; Bernasconi, M.; Goedecker, S.; Marx, D.; Tuckerman, M.; Parrinello, M., CPMD Program, MPI für Festkörperforschung and IBM Zurich Research Laboratory.

57. Grossman, J. C.; Schwegler, E.; Draeger, E. W.; Gygi, F.; Galli, G., Towards an assessment of the accuracy of density functional theory for first principles simulations of water. *J. Chem. Phys* **2004,** *120* (1), 300-311.

58. Sprik, M.; Hutter, J.; Parrinello, M., Ab initio molecular dynamics simulation of liquid water: Comparison of three gradient corrected density functionals. *J. Chem. Phys* **1996,** *105* (3), 1142-1152.

59. Troullier, N.; Martins, J. L., Efficient pseudopotentials for plane-wave calculations. *Phys. Rev. B* **1991,** *43* (3), 1993-2006.

60. Kleinman, L.; Bylander, D., Efficacious form for model pseudopotentials. *Phys. Rev. Lett.* **1982,** *48* (20), 1425-1428.

61. Sprik, M.; Ciccotti, G., Free energy from constrained molecular dynamics. *J. Chem. Phys* **1998,** *109* (18), 7737-7744.

Charts

1a **1b**

Chart 1 Tetraaquaberyllium cation **1a** and tetraammineberyllium cation **1b**

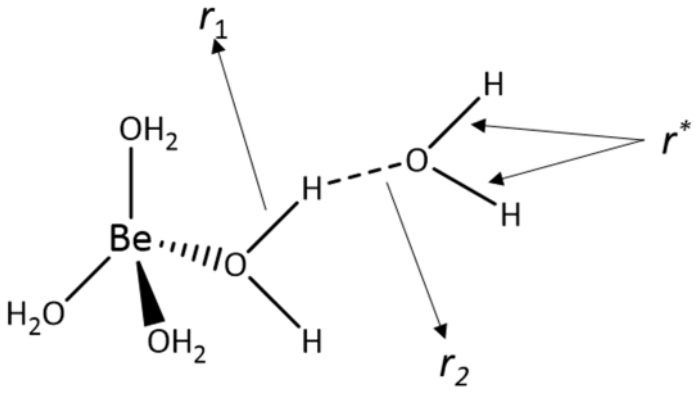

Chart 2 Tetraaquaberyllium cation **1a** solvated by a water molecule in the second solvation sphere revealing the O-H distances r_1 and r_2. (r* are the additional constraints imposed to prolong the reaction pathway)

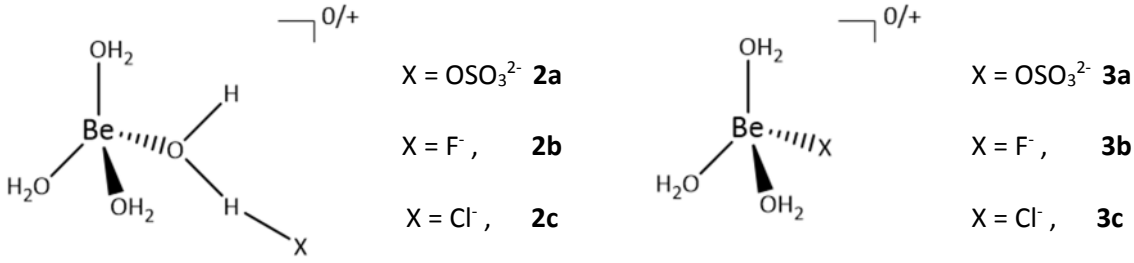

Chart 3 Outer sphere complexes (OSC) **2a-2c** and inner sphere complexes (ISC) **3a-3c** of beryllium complexes with sulfate, fluoride and chloride ions.

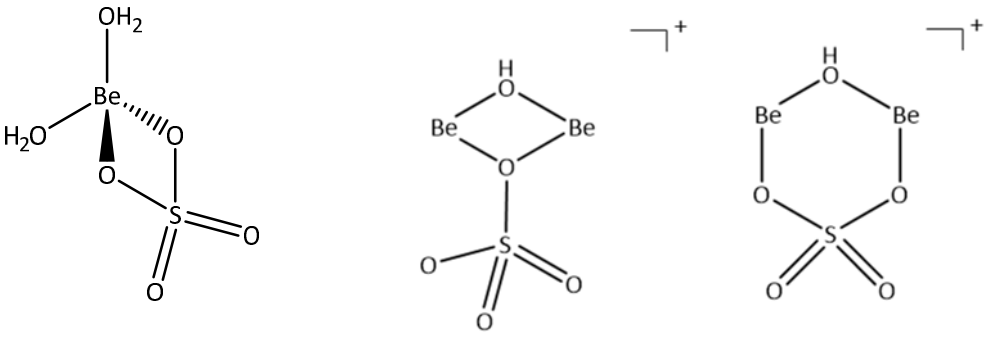

4a **4b** **4c**

Chart 4 Chelating or bridging coordination modes of the sulfato ligand

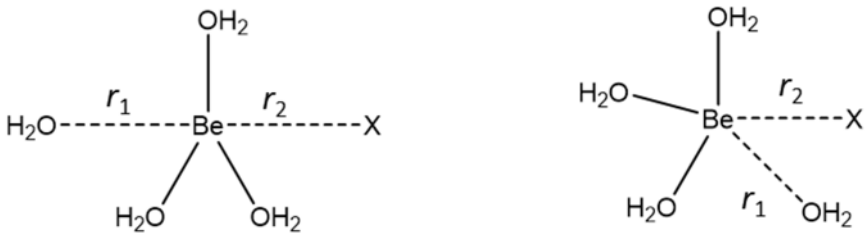

Chart 5 Transition state in a frontside and backside attack revealing O-Be-X constraint employed in the constrained CPMD simulation of the ligand substitution on the tetraaquaberyllium cation **1a**. ($\Delta r = r_1$-r_2 where r_1 = Be-X and r_2 = Be-O)

Figures

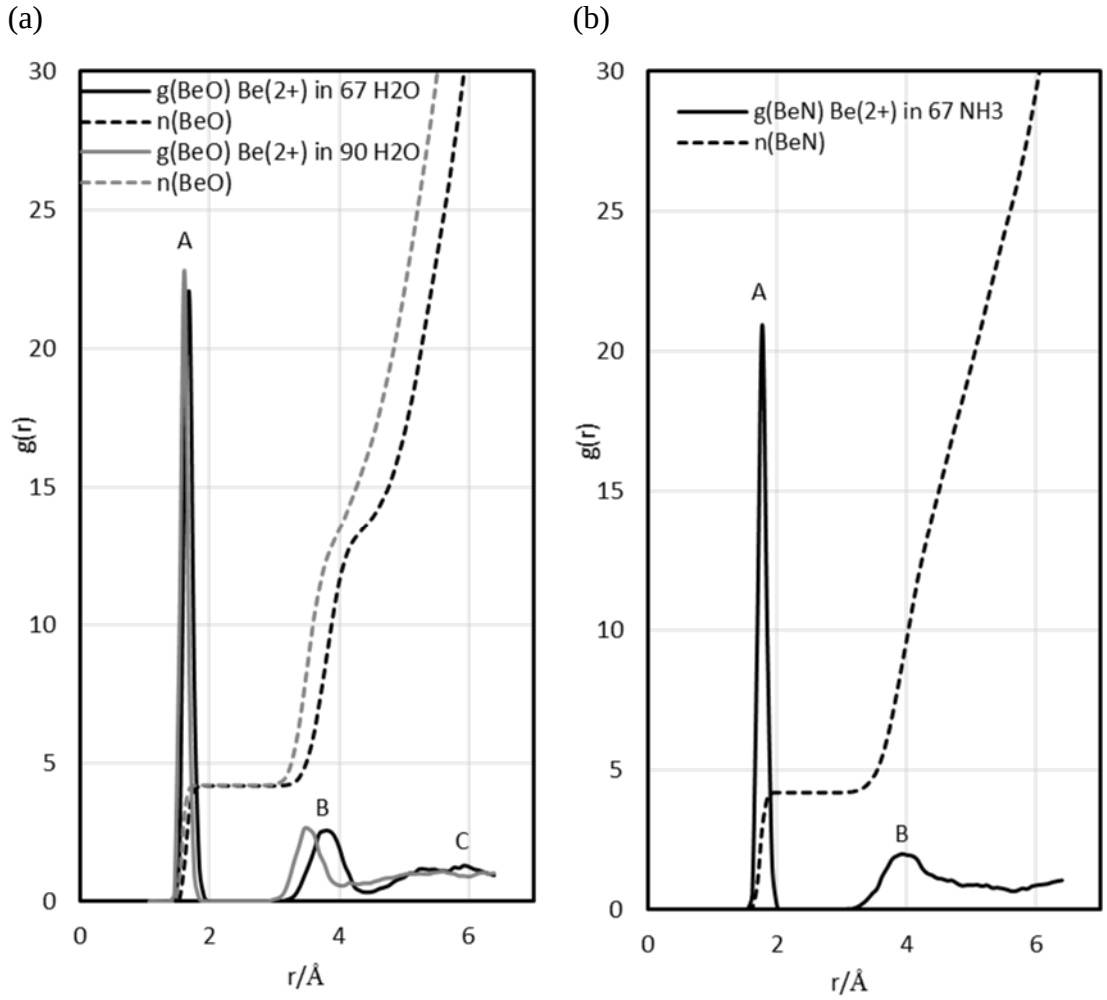

Figure 1 Solid lines: Be-O and Be-N radial distribution function of a) $[Be(H_2O)_4]^{2+}$ and b) $[Be(NH_3)_4]^{2+}$ in aqueous solution and liquid ammonia from unconstrained CPMD/BLYP simulations; dashed lines: total number of O or N atoms in a sphere with radius r around Be (data collected after the first 3 ps).

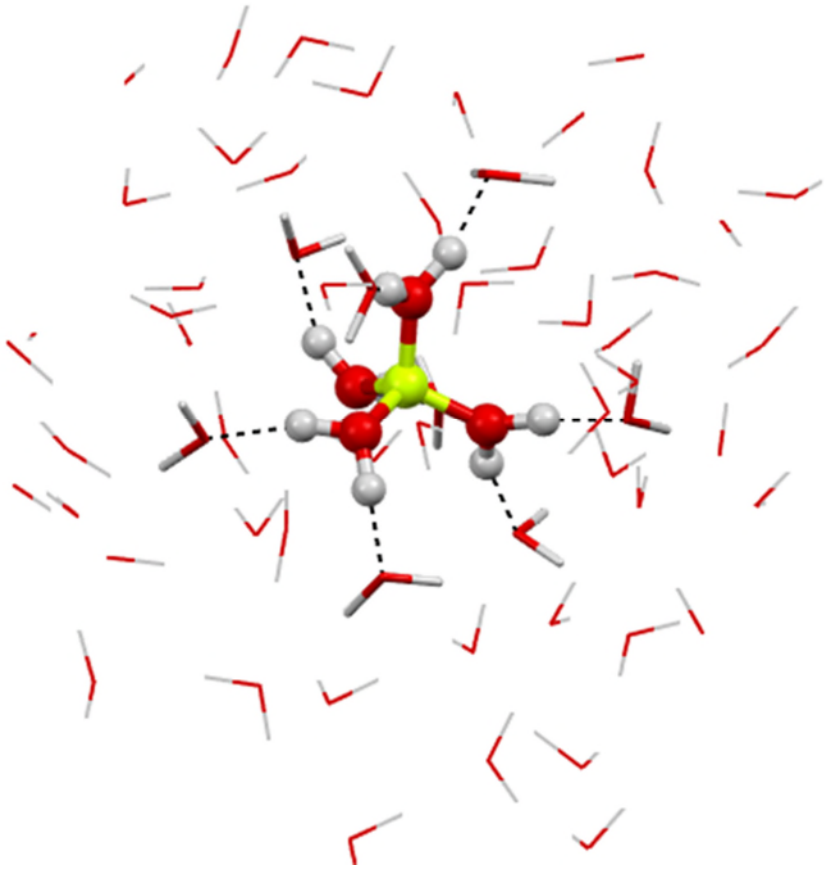

Figure 2 Snapshot showing the immediate coordination environment of the Be^{2+} ion revealing organisation of the primary solvation sphere (ball and stick model) and the hydrogen bonded network of secondary solvation sphere (tubes) from the CPMD simulation.

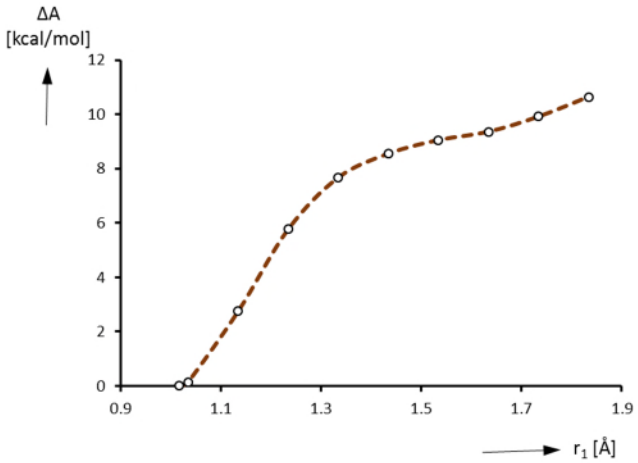

Figure 3 Computed free-energy profile for the deprotonation of the tetraaquaberyllium cation **1a** in aqueous solution.

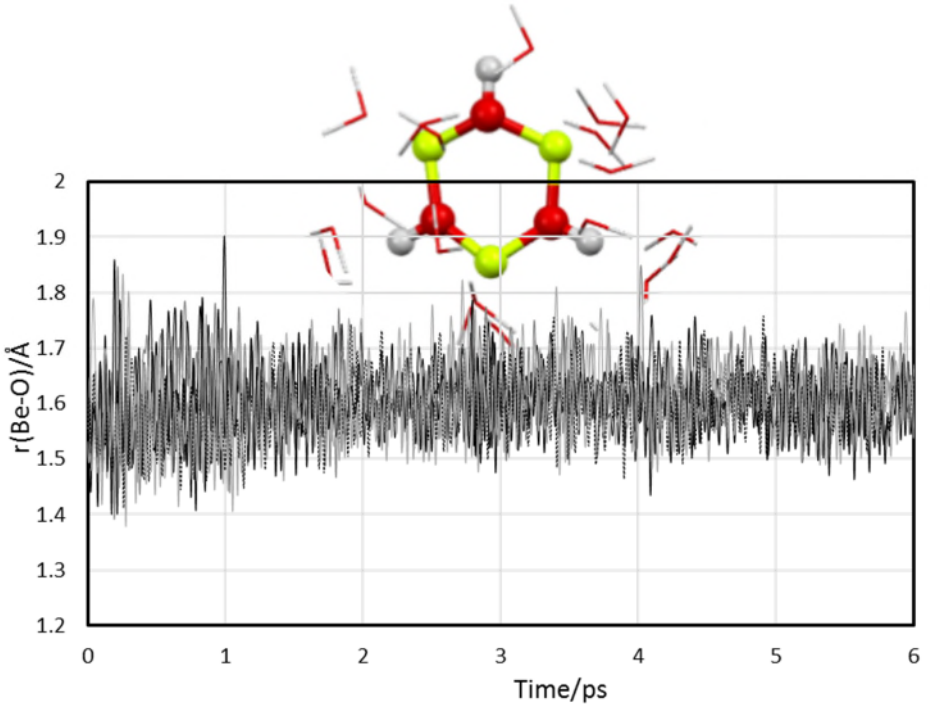

Figure 4 Time-evolution of Be-O distances (in Å) for the beryllium hydroxido trimer $[Be_3(OH)_3]^{3+}$ in aqueous solution for 6 ps (including representative snapshot from the 3 ps region)

(a) (b)

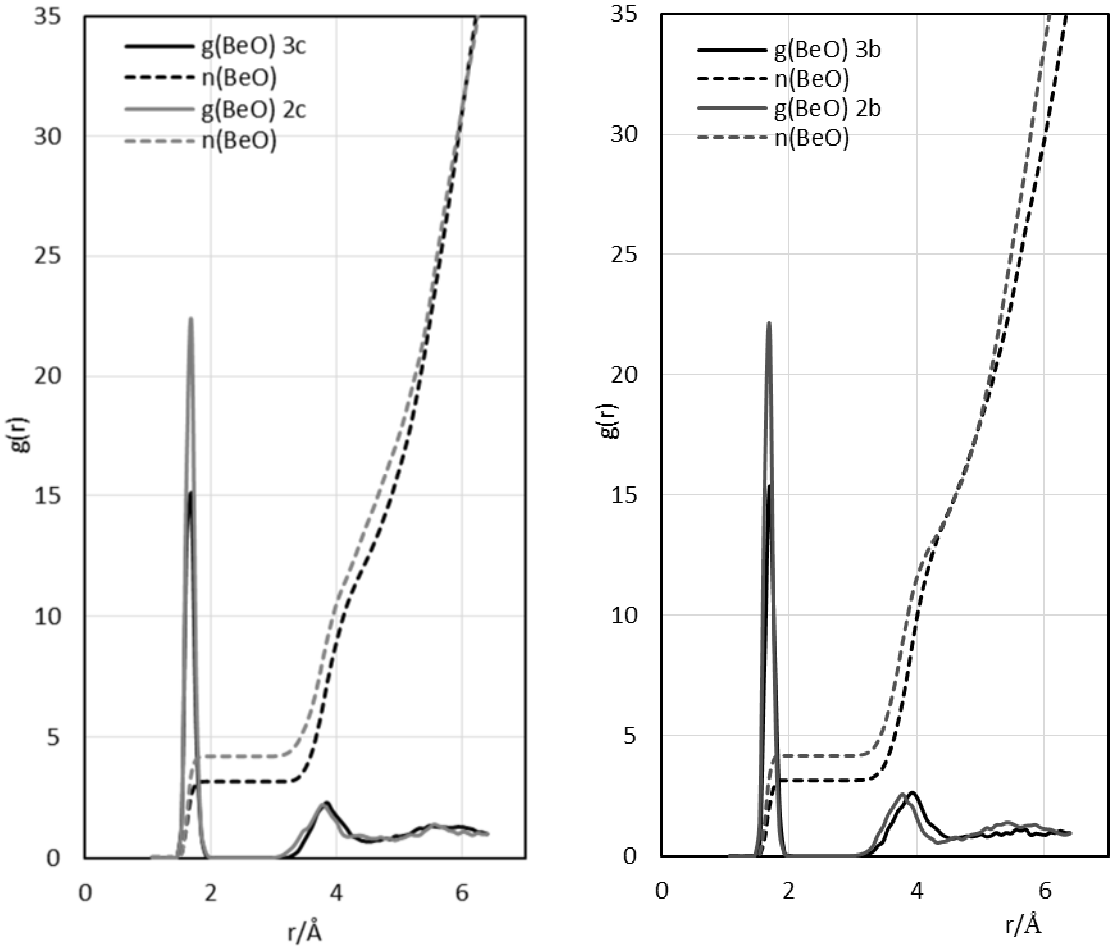

Figure 5 Be-O radial distribution function of a) beryllium chlorido complexes **2c** and **3c** b) beryllium fluorido complexes **2b** and **3b**.

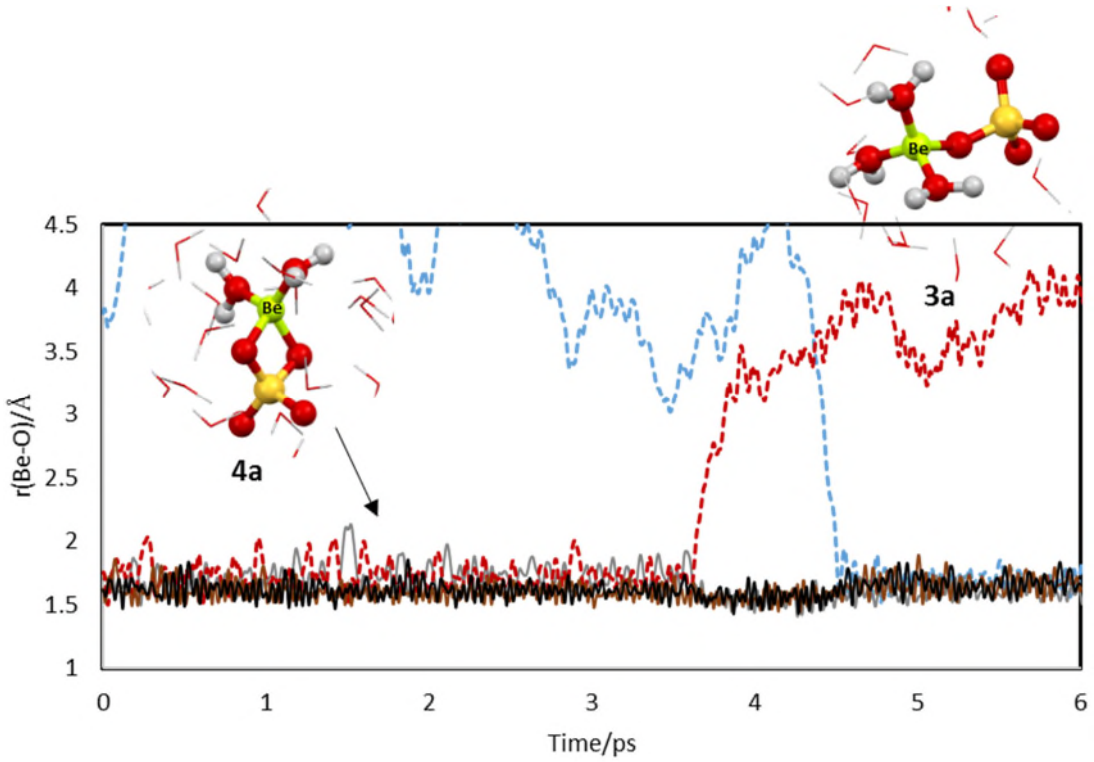

Figure 6 Time evolution of Be-O distances in complexes **4a** and **3a** (in Å) showing the lengthening of a Be-OSO_3 bond distance (red) and the entering of a water molecule into the primary coordination sphere (blue).

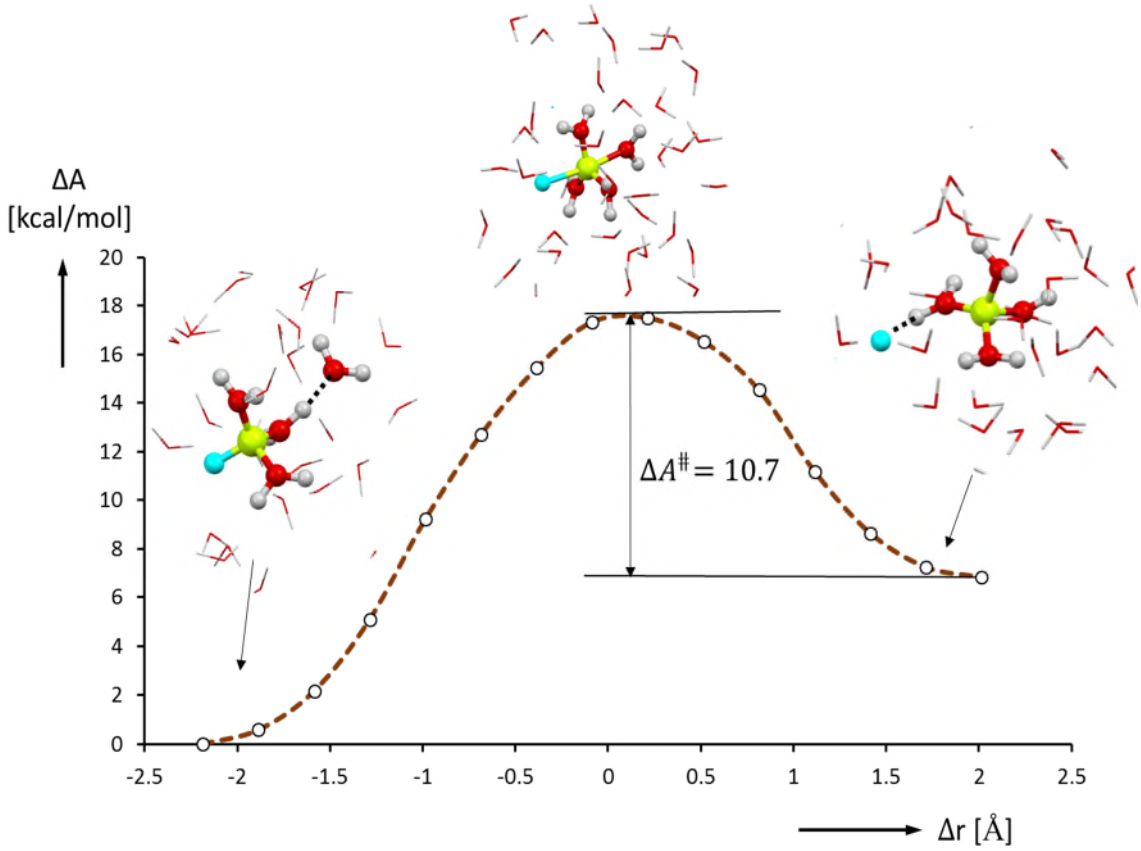

Figure 7 Calculated change in Helmholtz free energy, Δ*A*, for the substitution of an aqua ligand by a fluoride ion as obtained from constrained CPMD simulations and thermodynamic integration, including representative snapshots from the indicated region. (reaction coordinate: difference Δr between Be-O and Be-F bond distances).

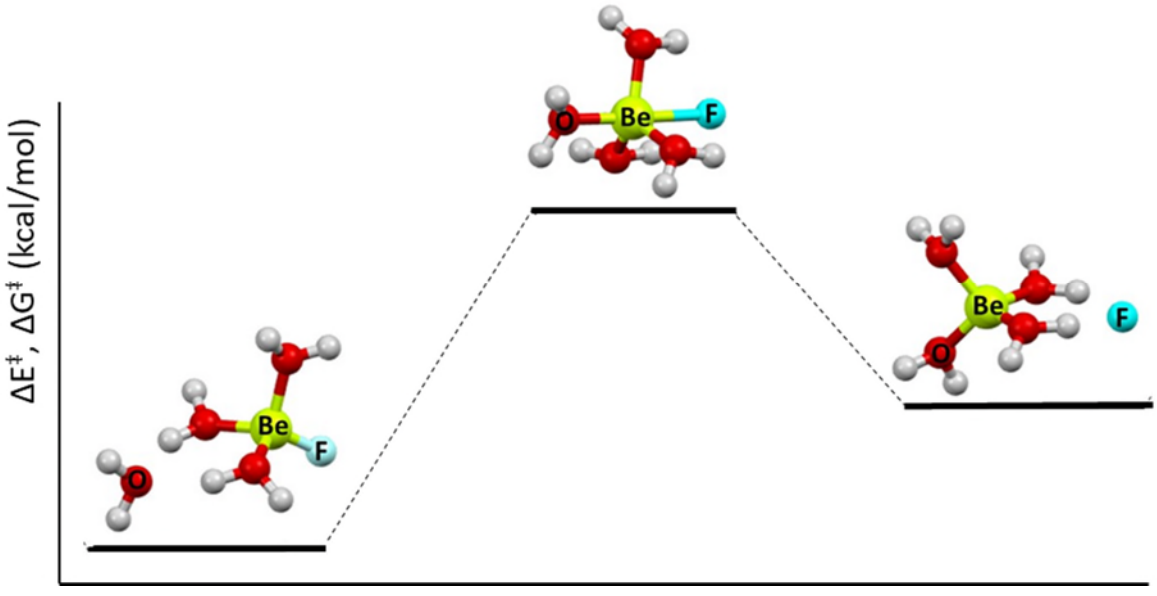

Figure 8 (Free) energy profile for the structural transition between the outer sphere and inner sphere structural arrangements of beryllium fluorido complex from static calculations (see Table 5 for selected values of $\Delta E^{\ddagger}$, $\Delta G^{\ddagger}$.).

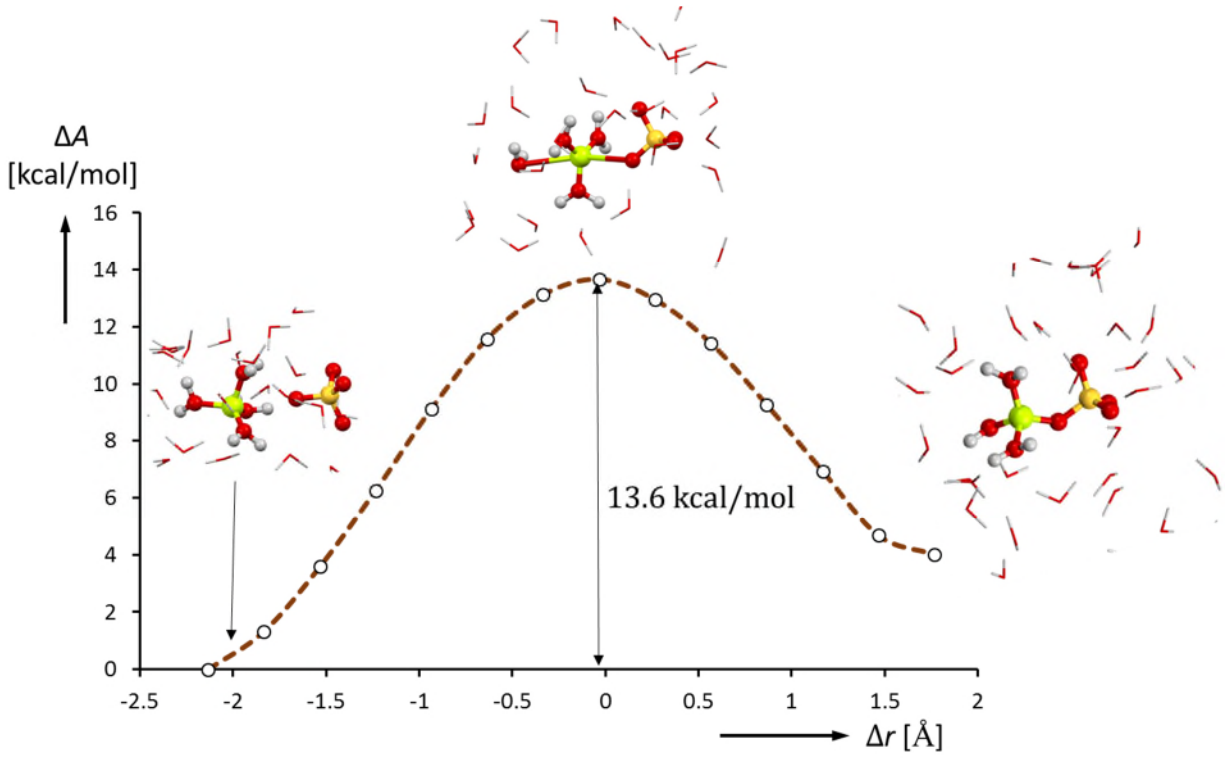

Figure 9a Calculated change in free energy, Δ*A*, for the substitution of an aqua ligand by a sulfato ligand as obtained from constrained CPMD simulations in aqueous solution and thermodynamic integration, including representative snapshots from the indicated region. (reaction coordinate: Be-OSO_3 bond distance).

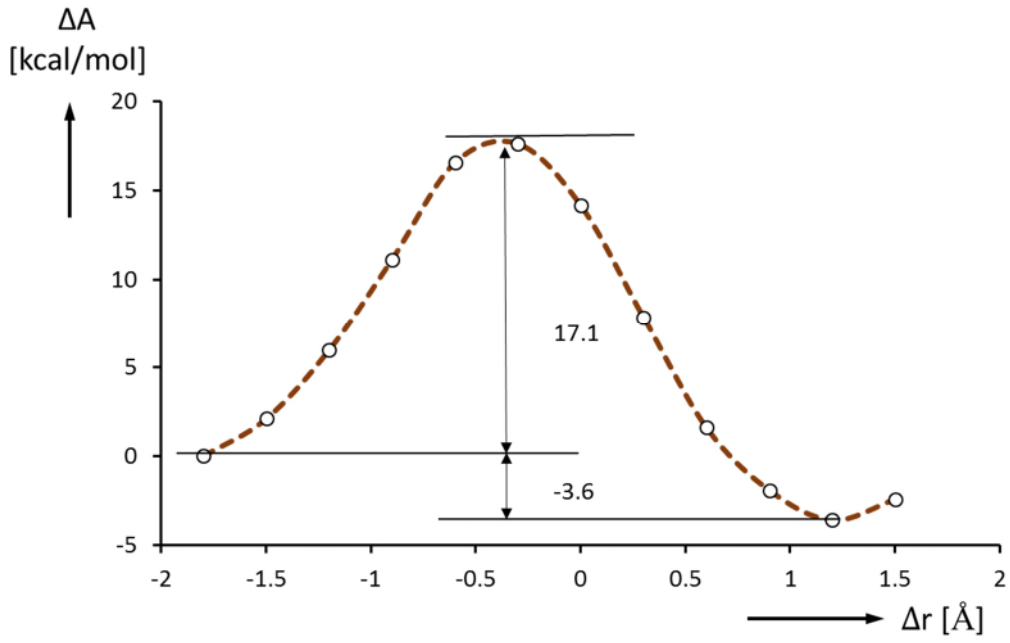

Figure 9b Calculated change in free energy, Δ*A*, for the substitution of an aqua ligand by a sulfato as obtained from constrained CPMD simulations in the gas phase and thermodynamic integration (reaction coordinate: Be-OSO_3 bond distance).

Table 1 Geometrical parameters (bond distances in Å) of complexes **2a-c**.

Type of complex	Comp.	Bond	BLYP	B3LYP[a]	B3LYP-D[a]3	MP2[a]	Cp-opt	$CPMD_{gas}$[b]	$CPMD_{aq}$[b]	Expt
Outer Sphere complex	**2a**	r(Be-O)	1.80	1.79[1.71]	1.76[1.71]	1.79[1.71]	1.77	1.80(6)	1.64(9)	1.60-1.69[c]
			1.78	1.77[1.71]	1.76[1.71]	1.77[1.70]	1.70	1.62(1)	1.66(23)	
			1.55	1.54[1.53]	1.56[1.53]	1.54[1.53]	1.51	1.51(27)	1.63(33)	
			1.57	1.54[1.64	1.53[1.64]	1.54[1.64]	1.65	1.71(61)	1.67(36)	
		r(Be···OSO_3)	3.01	3.41[3.57]	3.01[3.56]	3.39[3.51]	3.17	3.49(44)	3.99(86)	3.57[c]
	2b	r(Be-O)	1.71	1.70[1.65]	1.72[1.67]	1.72[1.68]	1.72	1.73(59)	1.64(11)	
			1.73	1.72[1.67]	1.70[1.68]	1.74[1.68]	1.73	1.73(9)	1.66(28)	
			1.68	1.51[1.55]	1.50[1.54]	1.69[1.68]	1.65	1.68(30)	1.63(11)	
			1.52	1.67[1.67]	1.67[1.68]	1.51[1.54]	1.52	1.52(15)	1.66(70)	
		r(Be-F)	3.08	3.06[3.12]	3.06[3.13]	3.12[3.14]	3.05	3.01(18)	3.61(15)	
	2c	r(Be-O)	1.66	1.64[1.62]	1.69[1.65]	1.65[1.65]	1.72	1.75(83)	1.64(64)	1.60-1.61[d]
			1.66	1.64[1.66]	1.69[1.65]	1.64[1.65]	1.65	1.73(66)	1.64(44)	
			1.66	1.64[1.62	1.60[1.63]	1.64[1.63]	1.73	1.68(67)	1.67(9)	
			1.67	1.66[1.66]	1.59[1.63]	1.64[1.63]	1.51	1.50(10)	1.65(0)	
		r(Be-Cl)	3.09	3.06[3.74]	3.41[3.65]	3.01[3.55]	3.55	3.60(23)	4.16(59)	

[a]Optimized equilibrium distances in the gas phase [in square brackets: values computed in a continuum solvation model (PCM)for the corresponding functional].[b]Mean distances in CMPD/BLYP simulations (in parentheses: standard deviations over the trajectories). [c]ref [7] (XRD, neutron and X-ray diffraction techniques). [d]ref [27]

Table 2 Geometrical parameters (bond distances in Å) of complexes **3a-c**, **4a**.

Type of complex	Comp.	Bond	BLYP	B3LYP[a]	B3LYP-D3[a]	MP2[a]	Cp-opt	$CPMD_{gas}$[b]	$CPMD_{aq}$[b]	Expt.
Inner Sphere complex	**3a**	r(Be-O) r(Be-OSO_3)	1.73 1.75 1.54 1.62	1.71[1.71] 1.73[1.67] 1.75[1.55] 1.53[1.64]	1.72 [1.71] 1.71 [1.67] 1.53 [1.55] 1.61 [1.64]	1.71 [1.67] 1.72 [1.71] 1.53 [1.55] 1.60 [1.64]	1.68 1.68 1.57 1.65	1.66(49) 1.71(02) 1.69(88) 1.56(33)	1.65(93) 1.67(12) 1.66(42) 1.63(27)	
	3b	r(Be-O) r(Be-F)	1.70 1.70 1.70 1.43	1.72[1.70] 1.71[1.70]] 1.68[1.70] 1.46[1.43]	1.70 [1.68] 1.67 [1.69] 1.70 [1.70] 1.46 [1.47]	1.71 [1.70] 1.66 [1.70] 1.71 [1.69] 1.44 [1.47]	1.71 1.70 1.70 1.42	1.73(04) 1.73(5) 1.73(3) 1.42(87)	1.66(31) 1.66(41) 1.69(81) 1.53(2)	
	3c	r(Be-O) r(Be-Cl)	1.70 1.70 1.70 1.88	1.70[1.70] 1.69[1.70] 1.70[1.70] 1.88[1.88]	1.70 [1.67] 1.70 [1.67] 1.70 [1.67] 1.88 [1.93]	1.70 [1.68] 1.70 [1.68] 1.70 [1.68] 1.86 [1.91]	1.69 1.71 1.69 1.89	1.72(8) 1.73(52) 1.73(43) 1.89(37)	1.65(82) 1.64(92) 1.63(53) 2.07(35)	 2.2[c]
	4a	r(Be-O) r(Be-O_2SO_2)	1.72 1.72 1.58 1.58	1.70[1.66] 1.70[1.66] 1.57[1.63] 1.57[1.63]	1.70 [1.63] 1.70 [1.63] 1.57 [1.66] 1.57 [1.66]	1.70 [1.63] 1.70 [1.63] 1.58 [1.66] 1.58 [1.66]	1.66 1.66 1.64 1.64	1.67 1.67 1.65 1.65		

[a]Optimized equilibrium distances in the gas phase [in square brackets: values computed in a continuum solvation model (PCM)for the corresponding functional].[b]Mean distances in CMPD/BLYP simulations (in parentheses: standard deviations over the trajectories).[c]EXAFS, ref [8]

Table 3 Computed energies according to equation (3) for the fluoride ion ($X=F^-$) in kcal/mol

	B3LYP			ΔG
n	ΔE (gas)	ΔE PCM	ΔG PCM	Expt[a]
1	-260.4	15.1	12.5	-6.68
2	-423.0	-19.0	-23.8	-5.13
3	-491.8	-65.9	-72.0	-3.8
4	-415.2	-59.3	-66.9	-1.94
	BLYP			ΔG
n	ΔE (gas)	ΔE PCM	ΔG PCM	Expt[a]
1	-256.4	17.76	15.1	-6.68
2	-415.3	-15.9	-19.9	-5.13
3	-481.1	-62.1	-68.5	-3.8
4	-401.1	-54.9	-62.9	-1.94

[a]ref 11

Table 4 Computed energies according to equation (3) for the chloride ion ($X=Cl^-$) in kcal/mol.

	B3LYP		
n	ΔE (gas)	ΔE PCM	ΔG PCM
1	-161.8	45.1	42.9
2	-335.4	37.9	34.2
3	-361.3	19.3	13.1
4	-299.2	36.8	28.6
	BLYP		
n	ΔE (gas)	ΔE PCM	ΔG PCM
1	-201.6	46.4	44.3
2	-310.8	38.8	34.5
3	-324.6	18.6	12.2
4	-249.5	36.3	27.7

Table 5 Computed activation energies for the transition between the outer sphere and inner sphere structural arrangements of beryllium fluorido complex (see Figure 8); energies and free energies of activation in kcal/mol.

Functional	$\Delta E^{\ddagger}$	$\Delta G^{\ddagger}$
B3LYP	12.3	12.7
BLYP	12.0	12.9
B3LYP-D3	12.1	12.5
MO6-2X	10.8	11.9
MP2	12.5	12.3

Graphical Abstract

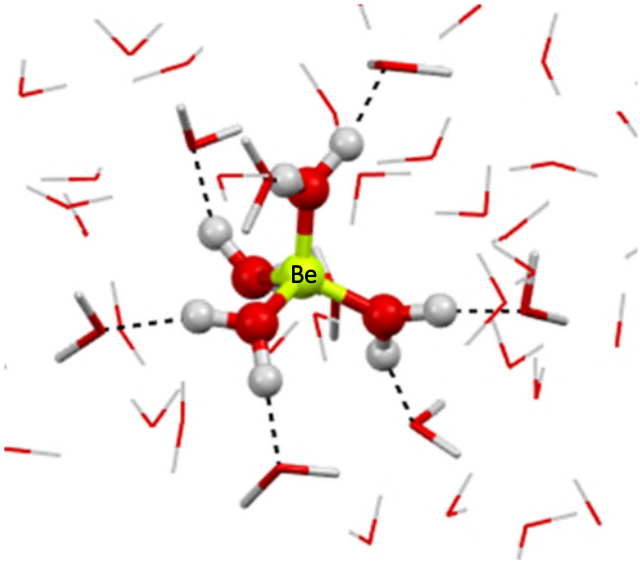

Synopsis

Ab initio nmolecular dynamic simulations are validated as tool to study structure and speciation of Be^{2+} complexes in aqueous solution